J. Fluid Mech. (1996), *vol.* 329, *pp.* 247–273

The stability of two-phase flow over a swept wing

By ADRIAN V. COWARD AND PHILIP HALL
Department of Mathematics, University of Manchester, Manchester M13 9PL, UK

(Received 19 October 1994 and in revised form 4 December 1995)

We use numerical and asymptotic techniques to study the stability of a two-phase air/water flow above a flat porous plate. This flow is a model of the boundary layer which forms on a yawed cylinder and can be used as a useful approximation to the air flow over swept wings. The air and water form an immiscible interface which can destabilize the flow, leading to travelling wave disturbances which move along the attachment line. This instability occurs for lower Reynolds numbers than is the case in the absence of a water layer. The two-fluid flow can be used as a crude model of the effect of heavy rain on the leading edge of a swept wing.

We also investigate the instability of inviscid stationary modes. We calculate the effective wavenumber and orientation of the stationary disturbance when the fluids have identical physical properties. Using perturbation methods we obtain corrections due to a small stratification in viscosity, thus quantifying the interfacial effects. Our analytical results are in agreement with the numerical solution which we obtain for arbitrary fluid properties.

1. Introduction

The laminar flow over an infinitely long cylinder can become unstable as the Reynolds number increases. When the axis of the cylinder is inclined at an angle relative to the free stream, the developed three-dimensional mean flow can be separated into two components, one lying in a plane normal to the axis, the other parallel to the generators of the cylinder. Small-amplitude disturbances to the flow can take the form of Tollmien–Schlichting waves, crossflow vortices, or Taylor–Görtler vortices (if there are regions of concave curvature).

The flow over a swept cylinder has been studied in detail, primarily because of its important application and relevance to the boundary layer which forms on the surface of swept wing. Understanding the mechanisms of flow instability for this model can lead to significant development of methods used in the reduction of laminar to turbulent flow transition.

The flow we study in this paper, is a classical Heimenz stagnation-point flow, together with a superposed non-zero component of velocity parallel to the axis. The equations governing the flow are written in Cartesian coordinates (see Prandtl 1946). The velocity component parallel to the axis of the cylinder can be determined independently by decoupling the momentum equations. The relevance of this solution to the realistic flow which forms on a swept wing is discussed in §3.2.

Using linear stability theory, Hall, Malik & Poll (1984) calculated critical Reynolds numbers for an infinite swept attachment-line boundary layer. They examined the effects of both suction and blowing at the boundary. Surface suction can be used as an effective laminar flow control since it thins the viscous boundary layer and leads

to a reduction in the local Reynolds number. In addition, the vorticity distribution is modified so that a more stable flow is established. Hall *et al.* obtained numerical and asymptotic results which clearly illustrate that even a small amount of suction can significantly stabilize the flow. Their results are in excellent agreement with the experimental investigations of Gaster (1967), Pfenninger & Bacon (1969) and Poll (1979, 1980). These authors investigated the stability of the attachment lines on swept wings and swept cylinders to small disturbances of naturally occurring frequences.

In 1986, Hall & Malik (1986) extended their linear stability results to include the nonlinear regime. The weakly nonlinear stability of this flow was examined using a Stuart–Watson expansion procedure. The primary motivation was to explain why experimental observations all correspond to modes near the lower branch of the neutral curve. Hall & Malik showed that apart from a small region near the critical Reynolds number, finite-amplitude solutions bifurcate from the upper branch when the Reynolds number is below the neutrally stable value elucidated from a linear stability analysis (subcritical). Equilibrium states associated with the upper branch are not therefore observed experimentally, since these solutions are unstable.

In addition these authors used numerical methods to integrate the time-dependent Navier–Stokes equations which govern the fully nonlinear problem. Using a Fourier–Chebyshev spectral method Hall & Malik found the existence of supercritical finite-amplitude states near the lower branch of the neutral curve.

Recently there has been much interest in the aerodynamic penalties associated with adverse weather conditions on aircraft flight. In a review of recent studies into the effects of heavy rain during take-off and landing, Dunham, Dunham & Bezos (1991) showed that short-duration, heavy precipitation can result in a premature loss of lift of 15–20 % and an increase in drag coefficient of up to 20%. It should be noted that these experiments were performed on two-dimensional airfoils for which there is no attachment line or crossflow instability.

The exact mechanisms which cause these detrimental flight characteristics are not clearly understood. Certainly the increased load on the wing will affect performance, but it is thought that other contributory mechanisms may also be active. One possible explanation is that when a thin water layer resides on the wing surface, the interface between the water and air layers may alter the stability of the flow. This interfacial mode could only play a role if a finite volume of water resides at the boundary. Clearly this could only occur during low-speed, low-altitude flight conditions, such as take-off or landing. With larger free-stream air flow the water layer would be forced out of the boundary layer, drying the surface of the wing. At higher altitudes, above dense cloud, rain is not a factor.

Interfacial instability arises in flows of two immiscible fluids which have differing fluid properties. In particular a viscosity jump across the fluid–fluid interface leads to a discontinuity in the velocity gradients due to continuity of tangential stress. Even flows which are stable to infinitely small disturbances (e.g. below the critical Reynolds number), can be destabilized by this mechanism, although the growth rate of the interfacial mode becomes asymptotically small as Reynolds number decreases.

Yih (1967) obtained asymptotic expressions for the growth rate of small-amplitude, long-wavelength perturbations to plane Couette and plane Poiseuille two-layer flow. When the fluid properties are identical, the interfacial mode is passive and, for plane Couette flow, these disturbances are linearly stable at all Reynolds numbers. For two fluids of different viscosities and/or densities interfacial instability is possible. The growth or decay of this mode depends on the many physical parameters and

geometry of the problem and incorporates surface tension forces, gravity, and volume ratios for example.

Since Yih's work, there have been numerous investigations of interfacial instability which have important applications in many situations. For example, Blennerhassett (1980) showed that the interfacial instability of air flow over water can lead to the generation of finite-amplitude waves. The effects of surface tension and gravity have been quantified in a variety of numerical and analytical studies which consider short-, moderate- and long-wavelength perturbations to the basic state (see Hooper & Boyd 1983, 1987; Hooper 1985 and Renardy 1985). The books by Joseph & Renardy (1993) give a comprehensive account of the many recent theoretical and experimental investigations of interfacial instabilities.

In this paper we consider a two-fluid analogue of the attachment-line boundary layer. We obtain an exact solution of the Navier–Stokes equations which govern the viscous two-phase flow. The domain consists of two separate regions. In the upper region of the boundary layer we have a two-dimensional stagnation-point flow together with a superposed crossflow component (due to the angle of inclination to the free stream). Below the air is a layer of water which, in the exact solution, forms an immiscible interface parallel to the boundary. In order to conduct an investigation of the interfacial mode we must assume that a constant depth of water lies in the lower layer. This restricts our attention to scenarios in which the drying effect of the air is balanced by the rate at which water enters the domain. This mechanism allows us to (crudely) consider the effect of heavy rain which is modelled by a flux of water being drawn into the lower layer. In §2 we obtain exact solutions for the base state. We note that in the absence of surface suction or blowing, a constant non-zero depth of water cannot be sustained. Thus we only consider flows in which the normal component of the velocity at the surface is non-zero.

In §3 we investigate the linear temporal stability of the flow to disturbances when the Reynolds number is finite. Since the basic flow is an exact solution of the Navier–Stokes equations, we are able to calculate the critical Reynolds numbers for a disturbance of arbitrary wavelength. By varying the viscosity and density ratios of the two fluids, we determine the stabilizing/destabilizing effect of the interfacial mode. We find that for both wall blowing and suction, the interface significantly destabilizes the flow. More precisely, we show that the flow is susceptible to travelling wave disturbances at lower Reynolds numbers than is the case for flow in the absence of a water layer.

The inviscid stability of a three-dimensional boundary layer was first comprehensively studied by Gregory, Stuart & Walker (1953). These authors used both experimental and theoretical techniques to develop an extensive understanding of the stability of the flow which forms on a rotating disk, and their findings have important consequences for the stability of general three-dimensional boundary layers.

The experimental work of Gregory *et al.* (1953) was based on the china-clay evaporation technique. They observed a regularly spaced pattern of equiangular spiral vortices which remain stationary, relative to the rotating disk. The angle made between these vortices and the radius vector of the disk was found to be in excellent agreement with the inviscid theory developed by Stuart. The prediction for the number of vortices was not, however, in such close agreement with the experimental observations. This discrepancy was attributed to viscous effects, and was resolved later when Hall (1986) used a self-consistent asymptotic theory to study the problem. Hall extended the inviscid analysis of Gregory *et al.* taking into account non-parallel flow effects. His results were consistent with those obtained by the parallel-flow

numerical investigation of Malik (1986), although this approximation is not valid at finite Reynolds numbers. In this work, Malik obtained a neutral curve for these stationary disturbances, and he also found a second stationary mode of instability which had been discovered experimentally by Federov *et al.* (1976).

In §4 we consider the inviscid stationary modes of instability of the flow described in §2. Using numerical methods we calculate the eigenvalues and eigenfunctions when the fluid properties are equated. We then compare these with our calculations for air flow over a water layer. In addition, we use asymptotic techniques for the case when the fluids have similar viscosities. This gives a useful method for quantifying the onset of the interfacial instability. We find that stationary modes are susceptible to interfacial effects due to a discontinuity in the shear stress at the unperturbed interface position. In §5 we draw some conclusions.

2. Formulation of the basic state

We consider the three-dimensional flow of two viscous, incompressible fluids above an infinite, horizontal, porous flat plate. The two fluids are immiscible and occupy separate regions. The upper-fluid velocity is denoted by $\boldsymbol{U}_1^*$ and the lower-fluid velocity by $\boldsymbol{U}_2^*$. We use Cartesian coordinates, with the (x^*, z^*)-axes lying in a plane parallel to the plate which is positioned at a vertical height $y^* = -d$. The porous plate allows us to model either the case of wall blowing, where there is a flux of fluid into the lower region, or wall suction where the normal velocity at the plate is in the $-y^*$ direction. The streamlines in the (x^*, y^*)-plane extend to infinity, the volume of fluid in each layer is then assumed to be constant and the interface between the two fluids is located at a height $y^* = \delta\eta^*(z^*, t^*)$ where η^* is an unknown function, and δ is constant.

The upper and lower fluids have viscosities μ_1, μ_2 and densities ρ_1 and ρ_2 respectively, so that the kinematic viscosities are $\nu_1 (= \mu_1/\rho_1)$ and $\nu_2 (= \mu_2/\rho_2)$. We define the fluid velocity and pressure to be

$$\boldsymbol{U}_{j=1,2}^* = \left[x^* U_j^*(y^*, z^*, t^*), V_j^*(y^*, z^*, t^*), W_j^*(y^*, z^*, t^*)\right], \tag{1}$$

$$P_{j=1,2}^* = P_j^*(y^*, z^*, t^*), \tag{2}$$

and the Navier–Stokes equations are

$$\frac{\partial U_j^*}{\partial t^*} + U_j^{*2} + V_j^* \frac{\partial U_j^*}{\partial y^*} + W_j^* \frac{\partial U_j^*}{\partial z^*} + \frac{1}{x^* \rho_j} \frac{\partial P_j^*}{\partial x^*} = \nu_j \nabla^2 U_j^*, \tag{3a}$$

$$\frac{\partial V_j^*}{\partial t^*} + V_j^* \frac{\partial V_j^*}{\partial y^*} + W_j^* \frac{\partial V_j^*}{\partial z^*} + \frac{\partial P_j^*}{\rho_j \partial y^*} = \nu_j \nabla^2 V_j^*, \tag{3b}$$

$$\frac{\partial W_j^*}{\partial t^*} + V_j^* \frac{\partial W_j^*}{\partial y^*} + W_j^* \frac{\partial W_j^*}{\partial z^*} + \frac{\partial P_j^*}{\rho_j \partial z^*} = \nu_j \nabla^2 W_j^*, \tag{3c}$$

$$U_j^* + \frac{\partial V_j^*}{\partial y^*} + \frac{\partial W_j^*}{\partial z^*} = 0. \tag{3d}$$

The Laplacian is defined as

$$\nabla^2(\cdot) \equiv \frac{\partial^2(\cdot)}{\partial y^{*2}} + \frac{\partial^2(\cdot)}{\partial z^{*2}},$$

and the subscript denotes the upper and lower fluids respectively. The form of the velocity and pressure fields (1) and (2) corresponds to an exact solution of the

momentum equations (3*a–d*), hence it is not necessary to make the boundary-layer approximation when deriving the basic flow, and in the subsequent analysis.

The tangential velocity of the lower fluid satisfies the no-slip boundary condition $(x^* U_2^*, W_2^*)\,(y^* = -d) = (0,0)$. The velocity perpendicular to the plate is prescribed by $V_2^*\,(y^* = -d) = V_0$, where $V_0 > 0$ corresponds to blowing, and $V_0 < 0$ represents suction at the wall.

The conditions far from the plate are given by

$$U_1^* \to \frac{U_0}{l}, \qquad W_1^* \to W_0 \qquad \text{as} \qquad y \to \infty.$$

Define $\Delta = (\mu_1 l/U_0\rho_1)^{1/2}$, l is a length scale in the streamwize direction and the velocity scale is W_0, so that

$$(x^*, y^*, z^*) = \Delta\,(X, Y, Z),$$
$$(x^* U^*, V^*, W^*) = W_0\,(XU, V, W).$$

Time t^*, and pressure $P_{j=1,2}^*$ are made dimensionless by Δ/W_0 and $\rho_1 W_0^2$ respectively. We also define the following non-dimensional parameters:

$$R_e = \frac{W_0 \Delta \rho_1}{\mu_1}, \quad \kappa = \frac{V_0 R_e}{W_0}, \quad D = \frac{d}{\Delta}, \quad m = \frac{\mu_2}{\mu_1}, \quad \rho = \frac{\rho_2}{\rho_1}, \quad \nu = \frac{\nu_2}{\nu_1}.$$

R_e is the Reynolds number, κ is the dimensionless normal velocity at the wall, and D is the depth of the lower fluid, scaled with respect to the length Δ. The parameters m, ρ and ν are the viscosity, density and kinematic viscosity ratios respectively.

At the interface between the upper and lower fluid layers, both velocity and tangential stress are continuous. The normal stress exhibits a discontinuous jump due to the effect of surface tension σ. Using the notation

$$[(\cdot)_j]_1^2 \equiv (\cdot)_2 - (\cdot)_1,$$

we obtain the following conditions which are applied at the non-dimensional interface position $Y = \delta\tilde{\eta}$:

$$[U_j]_1^2 = 0, \qquad [V_j]_1^2 = 0, \qquad [W_j]_1^2 = 0,$$

$$\left[2\mu_j \delta \frac{\partial \tilde{\eta}}{\partial Z}\left(\frac{\partial V_j}{\partial Y} - \frac{\partial W_j}{\partial Z}\right) + \mu_j\left(1 - \left(\delta\frac{\partial\tilde{\eta}}{\partial Z}\right)^2\right)\left(\frac{\partial W_j}{\partial Y} + \frac{\partial V_j}{\partial Z}\right)\right]_1^2 = 0,$$

$$\left[\mu_j \frac{\partial U_j}{\partial Y} - \delta\mu_j \frac{\partial\tilde{\eta}}{\partial Z}\frac{\partial U_j}{\partial Z}\right]_1^2 = 0,$$

$$\left[\mu_1 P_j\left(1 + \left(\delta\frac{\partial\tilde{\eta}}{\partial Z}\right)^2\right) - \frac{2\mu_j}{R_e}\frac{\partial V_j}{\partial Y} + \frac{2\mu_j\delta}{R_e}\frac{\partial\tilde{\eta}}{\partial Z}\left(\frac{\partial W_j}{\partial Y} + \frac{\partial V_j}{\partial Z}\right) - \frac{2\mu_j}{R_e}\frac{\partial W_j}{\partial Z}\left(\delta\frac{\partial\tilde{\eta}}{\partial Z}\right)^2\right]_1^2 - \mu_1 J\delta\frac{\partial^2\tilde{\eta}}{\partial Z^2}\left(1 + \left(\delta\frac{\partial\tilde{\eta}}{\partial Z}\right)^2\right)^{-1/2} = 0,$$

where $J = \sigma/\rho_1 W_0^2 \Delta$ is the non-dimensional surface tension coefficient. In addition, we must satisfy the kinematic condition

$$\frac{\mathrm{D}}{\mathrm{D}t}(Y - \delta\tilde{\eta}) = 0 \quad \Rightarrow \quad V_{j=1,2} = \delta\left(\frac{\partial\tilde{\eta}}{\partial t} + W_j\frac{\partial\tilde{\eta}}{\partial Z}\right) \qquad \text{at } Y = \delta\tilde{\eta}. \tag{4}$$

Let us now regard the flow in each region as a small perturbation of the basic state, so that with $\delta \ll 1$,

$$(XU, V, W)_{j=1,2} = \left(\frac{X\overline{U}}{R_e}, \frac{\overline{V}}{R_e}, \overline{W}\right)_j (Y) + \delta \left(X\tilde{U}, \tilde{V}, \tilde{W}\right)_j (Y, Z, t), \tag{5}$$

and the pressure is written in the form

$$P_{j=1,2} = -\frac{1}{2}\left(\frac{U_0 X \Delta}{l W_0}\right)^2 + \frac{\overline{P}_j}{R_e^2} + \delta \tilde{P}_j.$$

Note that since $\delta \ll 1$, the unperturbed interface position is $Y = 0$. We substitute this flow into the Navier–Stokes equations (3*a–d*), and take the limit $\delta \to 0$ to yield the following system of equations which determine the basic state:

$$\overline{U}_1 + \overline{V}_1' = 0, \tag{6a}$$

$$\overline{V}_1''' + \left(\overline{V}_1'\right)^2 - \overline{V}_1 \overline{V}_1'' - 1 = 0, \tag{6b}$$

$$\overline{W}_1'' - \overline{V}_1 \overline{W}_1' = 0, \tag{6c}$$

$$\overline{U}_2 + \overline{V}_2' = 0, \tag{7a}$$

$$\nu \overline{V}_2''' + \left(\overline{V}_2'\right)^2 - \overline{V}_2 \overline{V}_2'' - \rho^{-1} = 0, \tag{7b}$$

$$\nu \overline{W}_2'' - \overline{V}_2 \overline{W}_2' = 0. \tag{7c}$$

The boundary and interface conditions become

$$\overline{U}_2(-D) = \overline{W}_2(-D) = 0, \qquad \overline{V}_2(-D) = \kappa, \tag{8}$$

$$\overline{U}_1(\infty) = 1, \qquad \overline{W}_1(\infty) = 1, \tag{9}$$

$$\overline{U}_2(0) = \overline{U}_1(0), \qquad \overline{W}_2(0) = \overline{W}_1(0), \tag{10}$$

$$\overline{V}_2(0) = 0, \qquad \overline{V}_1(0) = 0, \tag{11}$$

$$m\overline{U}_2'(0) = \overline{U}_1'(0), \qquad m\overline{W}_2'(0) = \overline{W}_1'(0), \tag{12}$$

where $(\cdot)'$ denotes differentiation with respect to the normal coordinate Y.

Before finding a solution to the above equations, we firstly analyse the behaviour of the basic flow as $Y \to \infty$. For large Y, the asymptotic form for $\overline{V}_1$ and $\overline{W}_1$ can be expressed as

$$\overline{V}_1 = -\xi + \Gamma_0 \chi, \qquad \chi \ll 1, \tag{13a}$$

$$\overline{W}_1 = 1 - \lambda_0 \left[\frac{1}{\xi} + \Sigma\right] \exp\left(-\tfrac{1}{2}\xi^2\right), \tag{13b}$$

$$\Sigma = -\frac{1}{\xi^3} + \frac{3}{\xi^5} - \frac{15}{\xi^7} + \cdots + \frac{(-1)^n (2n-1)(2n-3)\cdots 3.1}{\xi^{2n+1}} + \cdots, \tag{13c}$$

where $\xi = Y + \tau$, $\chi = \chi(\xi)$ and τ, Γ_0 are constants (see Rosenhead 1963, Chapters V and VIII). After substitution into equations (6)–(7) we integrate with respect to Y to obtain the following asymptotic form for χ as $Y \to \infty$:

$$\chi = \tfrac{1}{3}\left[\chi'' + \xi \chi'\right],$$

$$\chi' = \frac{1}{2}\left[\frac{1}{\xi} + \Sigma + \xi^2 \Sigma\right] \exp\left(-\tfrac{1}{2}\xi^2\right),$$

$$\chi'' = \xi \Sigma \exp\left(-\tfrac{1}{2}\xi^2\right).$$

	Density (g cm^{-3})	Viscosity (g cm^{-1} s^{-1})	Kinematic viscosity (cm^2 s^{-1})
Air	1.225×10^{-3}	1.776×10^{-4}	1.450×10^{-1}
Water	9.991×10^{-1}	1.137×10^{-2}	1.138×10^{-2}
Water/Air	8.156×10^{2}	6.402×10^{1}	7.848×10^{-2}

TABLE 1. Physical properties of air and water.

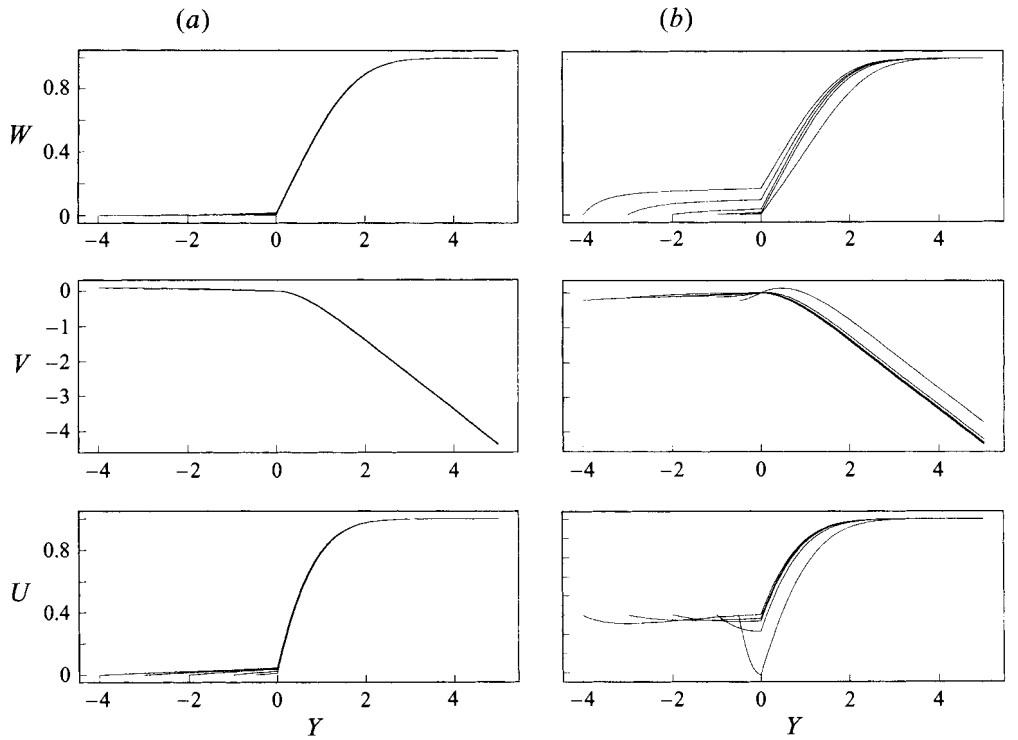

FIGURE 1. Basic flow of air over water: velocity profiles with (*a*) wall blowing and (*b*) wall suction, and water depth $D = 0.5, 1.2, 3, 4$.

Having derived expressions (13*a–c*) above, we obtain numerical values for the basic flow using a fourth-order Runge–Kutta scheme to integrate equations (6)–(7) with respect to Y, from Y_∞ to $-D$, where Y_∞ is an arbitrarily large number. Initial values for τ and Γ_0 were chosen, and then improved in order to satisfy the no-slip conditions (8) at the wall, and the kinematic condition (11) to within a specified tolerance. For the case of a single fluid ($m = 1 = \rho$) a step length of 1.0×10^{-5} gave excellent agreement with the results published in Rosenhead (1963, p. 232). To model the flow of air over water we obtain a solution of the system governing the basic state using the viscosity and density ratios shown in table 1 (see Batchelor 1967). The basic flow profiles $\overline{U}$, $\overline{V}$ and $\overline{W}$ are illustrated in figures 1(*a*) and 1(*b*) for blowing and suction respectively. Each figure shows the velocity components with depth of water $D = 0.5, 1, 2, 3$ and 4.

Given a constant depth of water D, we calculate the corresponding blowing or suction κ at the porous plate; the results are illustrated in figure 2(*a*). For the case

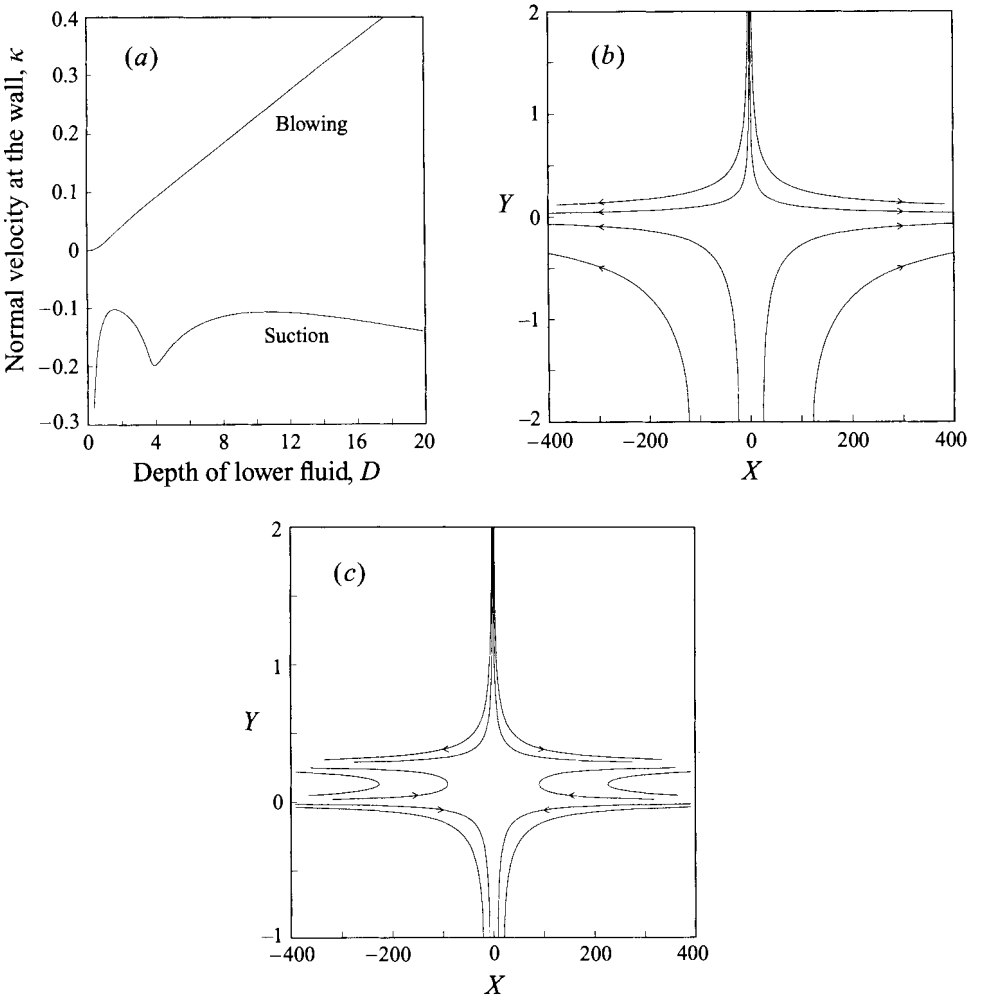

FIGURE 2. Basic flow of air over water: (*a*) water depth D and corresponding blowing/suction κ; (*b*) streamlines with wall blowing; (*c*) streamlines with wall suction.

$\kappa > 0$ (wall blowing), we see that the velocity at the plate increases almost linearly with depth of lower fluid D. With suction at the wall, the relationship is more involved.

In figure 2(*a*) we clearly see that when $\kappa = 0$ we obtain the somewhat degenerate solution with $D = 0$. This corresponds to the stagnation-point flow of air in the absence of a water layer below. An exact solution of the Navier–Stokes equations for a two-layer flow is is not possible if $\kappa = 0$. Equation (7), solved subject to homogeneous boundary/interface conditions (with $\kappa = 0$) yields the trivial solution in the lower layer. In the absence of suction or blowing, water is no longer drawn into the lower layer and the model breaks down. Physically this corresponds an aeronautical application where there is no mechanism drawing water into the boundary layer and the motion of the air drys the leading edge of the wing. As discussed previously, this restricts the validity of our model to applications of low-speed, low-altitude flight, for example during take-off or landing. For this reason, we only consider base flows for which the normal component of the velocity at the plate is non-zero.

Before we examine the flow stability, we first discuss the basic flow properties. The way in which a constant depth of lower fluid is maintained may not be immediately

obvious, especially in the case of wall suction. This is made clear by an analysis of the streamlines. By integrating $X\overline{U}_1$ and $X\overline{U}_2$ with respect to the normal coordinate Y we obtain figures 2(*b*) and 2(*c*) which show the streamlines at a particular location along the spanwize direction. We have chosen representative examples: $\kappa = 0.04$, $D = 2.0$; and $\kappa = -0.12$, $D = 1.0$. With a positive normal velocity at the plate, fluid enters the lower layer and moves towards a stagnation point at $X = 0 = Y$. The flow in the upper layer is directed towards the plate, in the $-Y$-direction. This is a classical Heimenz stagnation-point boundary-layer solution together with an imposed crossflow $\overline{W}$ acting in the spanwize direction.

For the case of suction, two stagnation points occur. There is a region above the interface (positioned at $Y = 0$), where $\overline{V}_1 > 0$ and $\overline{U}_1 < 0$ as shown by the velocity profiles in figures 1(*a*) and 1(*b*). The depth of this region increases with the suction, so that with a depth $D = 1.61$ and $\kappa = -0.1022$ (suction is a minimum here) the two stagnation points almost coincide. For $0 > Y > -D$ the flow is towards the porous plate where the tangential velocity satisfies the no-slip condition. At $Y = 0$ the kinematic condition (11) is imposed to prevent the transfer of fluid particles across the unperturbed interface (since the fluids are immiscible). The tangential velocity is continuous here although the gradient is discontinuous due to the viscosity ratio $m \neq 1$ (namely equation (12)).

The relationship between κ and D shown in figure 2(*a*) can be analysed as follows. For $\kappa \gg 1$ and $Y \sim O(1)$ equations (6)–(7) yield solutions

$$\overline{U}_2 = \frac{Y + D}{\rho\kappa} + \cdots,$$

$$\overline{V}_2 = \kappa - \frac{(Y + D)^2}{2\rho\kappa} + \cdots,$$

$$\overline{W}_2 = 1 - \exp\left[\frac{\rho(Y + D)\kappa}{m}\right] \cdots.$$

Imposing the kinematic condition $\overline{V}_2(Y = 0) = 0$ yields

$$D = (2\rho)^{1/2}\kappa \simeq 40.4\kappa,$$

which is in excellent agreement with the numerical values presented in figure 2(*a*).

For wall suction, the limit $\kappa \to -\infty$ corresponds to the singularity in the depth D. As $\kappa \to -\infty$, we see that $D \ll 1$, and momentum conservation in the spanwize direction suggests the use of the scaled variable

$$\zeta = \frac{(Y + D)|\kappa|\rho}{m},$$

so that for $\zeta \sim O(1)$

$$\overline{V}_2 \sim \kappa - \frac{m^2\zeta^2}{2\rho^3\kappa^3} + \cdots.$$

We now investigate the stability of the basic flow calculated above. We consider two distinct cases of physical interest: in §3 we look at the temporal stability of the flow when the Reynolds number is finite; in §4 we investigate inviscid stationary modes at high Reynolds numbers.

3. Viscous modes

The aim of this work is to quantify the effect of the interfacial viscosity and density stratification upon the stability of the basic flow when viscous effects are included. For a single fluid, linear and nonlinear stability analyses have shown that unstable disturbances propagate along the attachment line. The three-dimensional basic flow is independent of the spanwize coordinate Z (and is therefore an entirely parallel flow). Hence we employ periodic boundary conditions (in that direction) on the flow disturbances. Such methods cannot of course be used for flows which are spatially growing (non-parallel) such as the Blasius boundary layer which forms on a flat plate.

The flow described in the previous section is a first approximation to the boundary layer which forms on a swept wing, and is used to gain an understanding of the instability mechanisms which lead to transition from laminar to turbulent flow. To this end, we consider a convective instability in which disturbances propagate away from their source. For a discussion of absolute and convective instabilities the reader is referred to the review paper by Heurre & Monkewitz (1990). Following the work by Hall *et al.* (1984), we consider the temporal development of small-amplitude perturbations having a normal mode expansion

$$\left(\tilde{\eta}, \tilde{P}_{j=1,2}\right) = \left(\eta, P_{j=1,2}\right) \exp\left(\mathrm{i}k\,[Z - ct]\right), \tag{14a}$$

$$\left(\tilde{U}, \tilde{V}, \tilde{W}\right)_{j=1,2} = (U, V, W)_j \exp\left(\mathrm{i}k\,[Z - ct]\right). \tag{14b}$$

These perturbations are spatially periodic with wavelength $2\pi/k$ and with speed c.

The system of equations which govern the linearized stability problem is given by substituting equations (5) and (14) into the Navier–Stokes equations (3) and associated boundary/interface conditions and then discarding terms which are $o(\delta)$. We obtain

$$\mathrm{L}_1^2(U_1) = 2\overline{U}_1 U_1 + \overline{U}_1' V_1 + \overline{V}_1 U_1', \tag{15a}$$

$$\mathrm{L}_1^2(V_1) = R_e P_1' + \overline{V}_1' V_1 + \overline{V}_1 V_1', \tag{15b}$$

$$\mathrm{L}_1^2(W_1) = \mathrm{i}kR_e P_1 + \overline{V}_1 W_1' + R_e \overline{W}_1' V_1, \tag{15c}$$

$$U_1 + V_1' + ikW_1 = 0, \tag{15d}$$

$$\mathrm{L}_2^2(U_2) = 2\overline{U}_2 U_2 + \overline{U}_2' V_2 + \overline{V}_2 U_2', \tag{15e}$$

$$\mathrm{L}_2^2(V_2) = \frac{R_e P_2'}{\rho} + \overline{V}_2' V_2 + \overline{V}_2 V_2', \tag{15f}$$

$$\mathrm{L}_2^2(W_2) = \frac{\mathrm{i}kR_e P_2}{\rho} + \overline{V}_2 W_2' + R_e \overline{W}_2' V_2, \tag{15g}$$

$$U_2 + V_2' + \mathrm{i}kW_2 = 0, \tag{15h}$$

where

$$\mathrm{L}_1^2(\cdot) \equiv (\cdot)'' - k^2(\cdot) - \mathrm{i}kR_e\left(\overline{W}_1 - c\right)(\cdot),$$

$$\mathrm{L}_2^2(\cdot) \equiv \nu(\cdot)'' - \nu k^2(\cdot) - \mathrm{i}kR_e\left(\overline{W}_2 - c\right)(\cdot).$$

The velocity perturbation to the lower fluid satisfies the no-slip condition at the plate, and the conditions at the interface are obtained by expanding the velocity and stress components as Taylor expansions about the unperturbed interface position

$Y = 0$:

$$U_2 + \eta\frac{\overline{U}_2'}{R_e} = U_1 + \eta\frac{\overline{U}_1'}{R_e},$$

$$V_2 + \eta\frac{\overline{V}_2'}{R_e} = V_1 + \eta\frac{\overline{V}_1'}{R_e},$$

$$W_2 + \eta\overline{W}_2' = W_1 + \eta\overline{W}_1',$$

$$m\left(\frac{2ik\eta\overline{V}_2'}{R_e} + \overline{W}_2''\eta + ikV_2 + W_2'\right) = \frac{2ik\eta\overline{V}_1'}{R_e} + \overline{W}_1''\eta + ikV_1 + W_1',$$

$$m\left(\frac{\eta\overline{U}_2''}{R_e} + U_2'\right) = \frac{\eta\overline{U}_1''}{R_e} + U_1',$$

$$P_2 + \frac{\eta\overline{P}_2'}{R_e^2} - m\left(\frac{2\eta\overline{V}_2''}{R_e^2} + \frac{2V_2'}{R_e}\right) = P_1 + \frac{\eta\overline{P}_1'}{R_e^2} - \frac{2\eta\overline{V}_1''}{R_e^2} - \frac{2V_1'}{R_e} - k^2\eta J.$$

The kinematic condition (4) becomes

$$\eta = \frac{R_e V_1}{ikR_e\left(\overline{W}_1 - c\right) - \overline{V}_1'}. \tag{16}$$

The upper fluid velocity $\boldsymbol{U}_1$ must match the undisturbed flow as we move far away from the plate; we therefore require the perturbed flow to decay exponentially as Y becomes large. Hall *et al.* (1984) showed that by replacing the basic flow by its asymptotic dependence for $Y \gg 1$ (equation (13)), the perturbed velocity in the upper fluid has the form

$$\left.\begin{aligned} U_1 &\sim W_1 \sim \exp\left(-Y^2/2\right) \\ V_1 &\sim \exp\left(-kY\right) \end{aligned}\right\} \quad \text{as } Y \to \infty.$$

Equations (15*a–h*) govern the stability of the lower fluid and are defined on the domain $-D \leqslant Y \leqslant \delta\eta$, whilst those for the upper fluid are defined for $\delta\eta \leqslant Y \leqslant \infty$. These equations in general require a numerical solution.

For a given Reynolds number R_e, and real wavenumber k, we obtain the corresponding complex eigenvalue c. The imaginary part, denoted c_i, determines kc_i, the linear temporal growth or decay of the perturbation to the basic state. When $c_i > 0$ the flow is said to be linearly unstable and for $c_i < 0$ it is linearly stable.

3.1. *Numerical solution*

Solving the stability problem by means of a standard shooting method becomes prohibitively expensive as the Reynolds number increases. The rapidly varying nature of the eigenfunctions results in a loss of independence of orthogonal solutions due to the introduction of a 'parasitic' error at each integration step. High accuracy can only be guaranteed if the step length is made vanishingly small. These difficulties were overcome by implementing a compact fourth-order finite difference scheme of the form developed by Malik, Chuang & Hussaini (1982). This method was later used by Hall *et al.* (1984) to investigate the attachment-line stability of a single fluid; a detailed account of the implementation of this scheme is given by these authors. The

method is applicable to a set of linear first-order ordinary differential equations with an equal number of boundary conditions prescribed at each end of the domain. Our solution strategy is as follows: the equations describing the stability problem above have been formulated as two sixth-order ordinary differential systems with coupled interface conditions. We define two column vectors

$$\psi_{j=1,2} = \left(\phi_{1j}, \phi_{2j}, \phi_{3j}, \phi_{4j}, \phi_{5j}, \phi_{6j}\right)^T = \left(U_j, V_j, W_j, P_j, U_j', W_j'\right)^T,$$

where, as before, the subscript $j = 1, 2$ denotes the upper and lower fluids respectively, and T denotes the transpose of the vector. The equations can now be formulated as twelve first-order linear differential equations such that

$$\frac{\mathrm{d}\phi_{lj}}{\mathrm{d}Y} = \sum_{n=1}^{6} (a_{ln})_j \phi_{nj}, \qquad l = 1, 2, \ldots 6, \quad j = 1, 2,$$

$$\frac{\mathrm{d}^2\phi_{lj}}{\mathrm{d}Y^2} = \sum_{n=1}^{6} (b_{ln})_j \phi_{nj}, \qquad l = 1, 2, \ldots 6, \quad j = 1, 2,$$

$$b_{ln} = \frac{\mathrm{d}a_{ln}}{\mathrm{d}Y} + \sum_{p=1}^{6} a_{lp} a_{pn}.$$

Defining $f_2 = k^2 m \rho^{-1} + \mathrm{i}k(\overline{W}_2 - c)R_e$, we find that the 6×6 matrix $(a_{ln})_2$ has the following non-zero elements:

$$\begin{aligned}
&(a_{15})_2 = 1, && (a_{21})_2 = -1, && (a_{23})_2 = -\mathrm{i}k,\\
&(a_{36})_2 = 1, && (a_{41})_2 = \rho \overline{V}_2 R_e^{-1}, && (a_{42})_2 = -\rho R_e^{-1}\left(f_2 + \overline{V}_2'\right),\\
&(a_{43})_2 = \mathrm{i}k\rho \overline{V}_2 R_e^{-1}, && (a_{45})_2 = -m R_e^{-1}, && (a_{46})_2 = -\mathrm{i}k m R_e^{-1},\\
&(a_{51})_2 = \rho m^{-1}\left(f_2 + 2\overline{U}_2\right), && (a_{52})_2 = \rho m^{-1}\overline{U}_2', && (a_{55})_2 = \rho m^{-1}\overline{V}_2,\\
&(a_{62})_2 = \rho m^{-1} R_e \overline{W}_2', && (a_{63})_2 = \rho m^{-1} f_2, && (a_{64})_2 = \mathrm{i}k m^{-1} R_e,\\
&(a_{66})_2 = \rho m^{-1}\overline{V}_2.
\end{aligned}$$

The corresponding matrix $(a_{ln})_1$ is obtained from the above by setting m and ρ to unity. The numerical method is then derived using the Euler–Maclaurin formulae

$$\psi_j^n = \left(\phi_1^n, \phi_2^n, \ldots \phi_6^n\right)_j^T = \psi_j(Y_n), \tag{17}$$

$$h_n = Y_n - Y_{n-1}, \tag{18}$$

$$\psi_j^n - \psi_j^{n-1} = \frac{h_n}{2}\left(\frac{\mathrm{d}\psi_j^n}{\mathrm{d}Y} + \frac{\mathrm{d}\psi_j^{n-1}}{\mathrm{d}Y}\right) - \frac{h_n^2}{12}\left(\frac{\mathrm{d}^2\psi_j^n}{\mathrm{d}Y^2} - \frac{\mathrm{d}^2\psi_j^{n-1}}{\mathrm{d}Y^2}\right) + O\left(h_n^5\right). \tag{19}$$

The nodes are distributed so that in the upper fluid

$$g_1 = \frac{Y_\infty + \mathrm{L}_1}{Y_\infty},$$

$$Y_n = \frac{\mathrm{L}_1 (n-1)}{N g_1 - (n-1)}, \qquad n = 1, 2, \ldots, N+1,$$

where $N + 1$ is the total number of nodes, Y_∞ is the edge of the boundary layer, and the scaling parameter chosen such that $\overline{W}_1\left(\mathrm{L}_1/2\right) = 0.5$. Malik *et al.* (1982) showed

that such a choice of L_1 yielded maximum accuracy. Similarly in the lower fluid layer

$$g_2 = \frac{D + \mathrm{L}_2}{D},$$

$$Y_n = \frac{\mathrm{L}_2 (n-1)}{Mg_2 - (n-1)}, \qquad n = 1, 2, \ldots, M+1,$$

such that $\overline{W}_2 (\mathrm{L}_2/2) = \kappa/2$.

For both the upper and lower fluids, equation (19) becomes

$$\phi_l^n - \phi_l^{n-1} - \frac{h_n}{2} \sum_{p=1}^{6} a_{lp}^n \phi_p^n + \frac{h_n^2}{12} \sum_{p=1}^{6} b_{lp}^n \phi_p^n - \frac{h_n}{2} \sum_{p=1}^{6} a_{lp}^{n-1} \phi_p^{n-1}$$

$$- \frac{h_n^2}{12} \sum_{p=1}^{6} b_{lp}^{n-1} \phi_p^{n-1} = 0, \qquad n = 2, \ldots, N+1, \qquad l = 1, 2, \ldots 6,$$

which may be written in block-tridiagonal form so that the solution across each fluid layer is obtained efficiently. To this end, we introduce independent inhomogeneous velocity components at the interface, and equation (16) gives the corresponding interfacial deformation η. We find a suitable linear combination of these three independent solutions, so that for a specified lower fluid depth D, Reynolds number R_e, and wavenumber k, the conditions of stress continuity at $Y = 0$ are satisfied, and the complex eigenvalue c is obtained. When we equate the densities and viscosities of the two fluids, the numerical scheme yields exactly the eigenvalues found by Hall *et al.* (1984). When the imaginary part of the eigenvalue c is zero, there is no temporal growth or decay of the disturbance to the basic state, and the flow is neutrally stable. We then iterate to obtain neutral disturbances characterized by $c_i = 0$. Figure 3 shows four neutral curves: an impermeable plate with $\kappa = 0$; wall blowing with $\kappa = 0.137$ and $\kappa = 0.4$; and with suction $\kappa = -0.1$. Inside the curves, c has a positive imaginary part and the perturbations (U_j, V_j, W_j, η) grow exponentially in time.

The eigenvectors given in figure 4(*a–c*) have been normalized so that the maximum magnitude of each velocity component is unity. Figure 4(*a*) shows both real and imaginary parts of the three velocity components when the fluid viscosities and densities are equal. It has been verified that these (and other) eigenvectors are the same as those published by Hall *et al.* (1984). In figures 4(*b*, *c*) we clearly see the discontinuities in the velocity and shear stress at the unperturbed interface position $Y = 0$ which is due to the difference in viscosities and densities of the air and water layers. It is this discontinuity that plays an important role in altering the stability of the flow. The neutral curves for air flow over water are drawn in the (k, R_e)-plane. Figures 5(*a*) and 5(*b*) correspond to cases of wall blowing and suction respectively. These results are discussed in the following section.

3.2. *Discussion*

Before we discuss the novel results of our numerical calculations we first comment on the relevance of the exact solution to the actual flow which forms on swept wings and swept cylinders. The boundary layer flow over a yawed, infinitely long cylinder was investigated and by Sears (1948), (and in the unpublished work of Schubart). Their work is discussed in Chapter VIII of Rosenhead (1963). Using Cartesian coordinates, the velocity components are expanded in powers of x/l, where x is the distance measured along the surface perpendicular to the cylinder generators and l

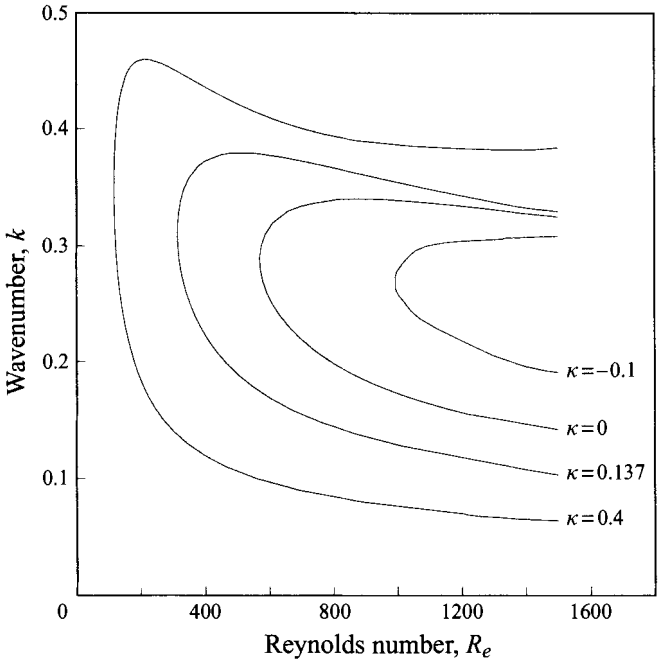

FIGURE 3. Neutral curves with equal viscosities and densities: impermeable plate $\kappa = 0$, blowing with $\kappa = 0.137$ and $\kappa = 0.4$, and suction with $\kappa = -0.1$.

is an appropriate length-scale. Close to the leading edge of the cylinder, and for a sufficiently large radius of curvature, the effects of curvature can be assumed negligible. The leading-order solution (higher powers of x/l are ignored) reduces identically to the flow that we have calculated in §2. The accuracy of this approximation depends, therefore, on the geometry of the cylinder or swept wing. Results using this model will be most relevant to wing sections which have a flat nose.

Since the basic flow is only a first approximation to the flow near the attachment line, asymptotic methods based on a high-Reynolds-number assumption must be used to investigate the practical problem. In addition, the two-fluid flow studied here is not an exact representation of the actual effects of heavy rain on the leading edge of a swept wing. A more applicable model would need to incorporate a more realistic mechanism by which rain can enter the boundary layer. In addition our model restricts our study to a situation in which a constant depth of water is sustained in the base flow. In practice this may only occur over a relatively short period of time. However, this analysis does highlight the potential effects of interfacial instability which may be a contributory factor in the overall deterioration in flight characteristics experienced in adverse weather conditions.

It is worth making a few comments about the dimensional quantities in this problem. The velocity components in each fluid are made dimensionless using the spanwise free-stream speed W_0. The length scale $\Delta = (\mu_1 l/U_0\rho_1)^{1/2}$ is based on the streamwise velocity U_0 and length l. In a practical situation then, the density and viscosity of the water and air would be fixed parameters (given in table 1), as would the normal velocity at the surface, V_0. We have shown in the previous section that with a given value of κ (the dimensionless parameter quantifying the amount of blowing or suction) we can calculate the corresponding non-dimensional depth of water D. The actual height of the interface is therefore not a free parameter and is

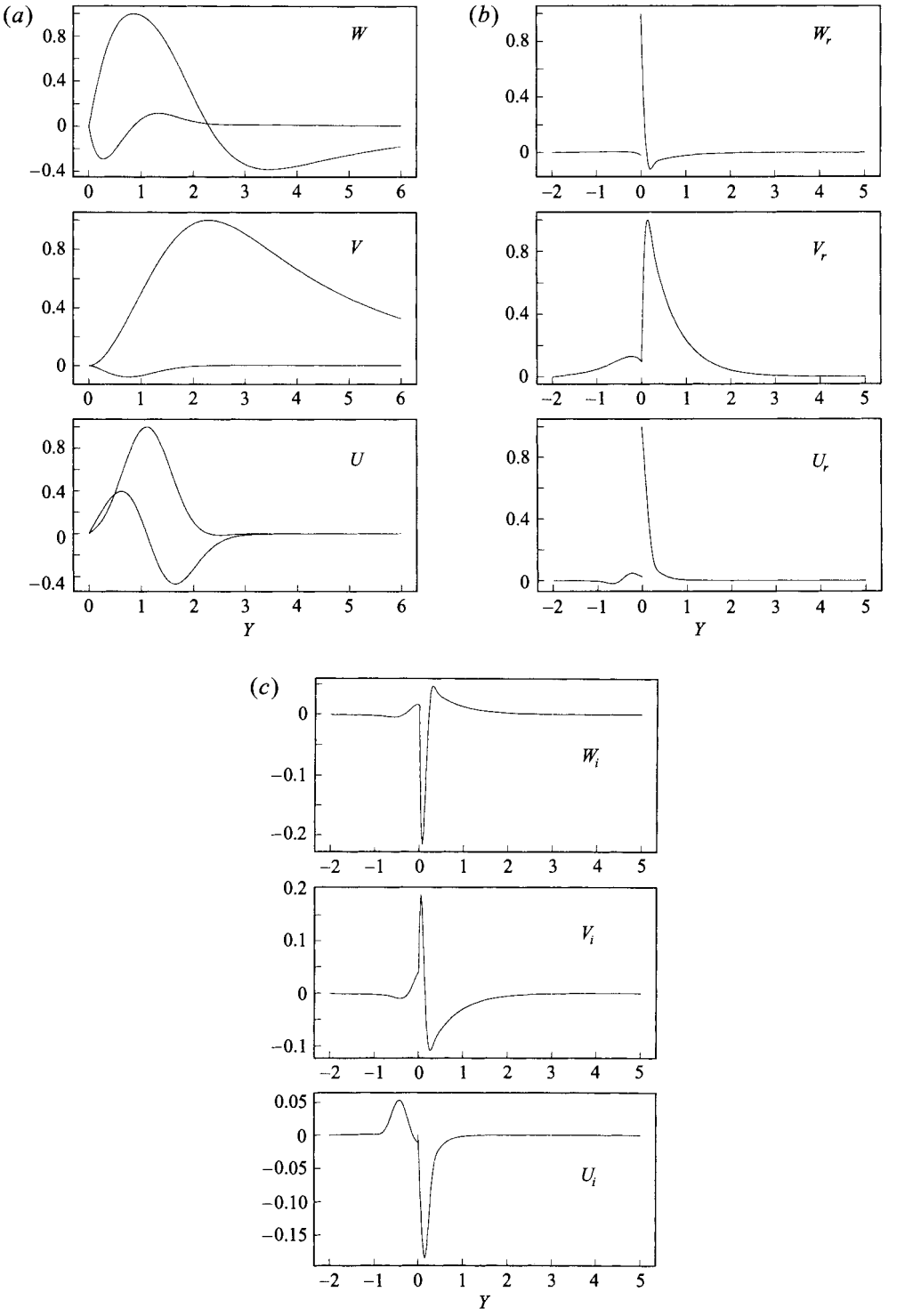

FIGURE 4. (*a*) Neutral eigenfunctions U, V, W for a single fluid, $R_e = 119$, $\kappa = 0.4$ (*b*) Real part and (*c*) imaginary part of neutral eigenfunctions U, V, W for air flow over water, $R_e = 1580$, $\kappa = 0.04$.

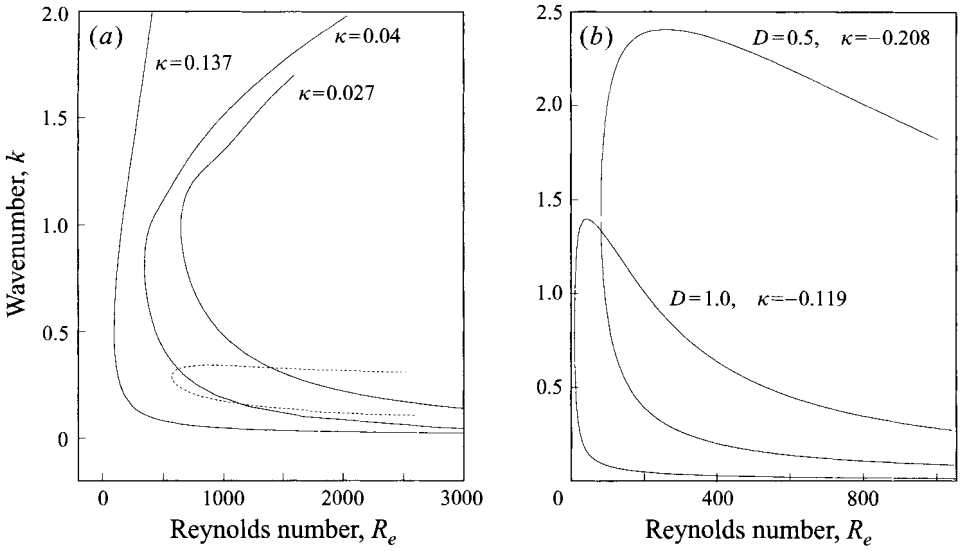

FIGURE 5. Neutral curves: (*a*) solid lines correspond to the flow of air over water with increasing wall blowing; dotted line shows the neutral curve for a single fluid with no wall blowing. (*b*) the stability of air flow over water with suction at the wall.

N	k	Re $\{kc\}$	κ
10	3.300581×10^{-1}	1.226919×10^{-1}	0.0
20	3.378719×10^{-1}	1.267951×10^{-1}	0.0
40	3.384238×10^{-1}	1.270776×10^{-1}	0.0
80	3.384613×10^{-1}	1.270965×10^{-1}	0.0
160	3.384638×10^{-1}	1.270977×10^{-1}	0.0
10	8.540221×10^{-2}	2.284554×10^{-2}	0.4
20	8.428938×10^{-2}	2.243776×10^{-2}	0.4
40	8.415787×10^{-2}	2.238444×10^{-2}	0.4
80	8.414404×10^{-2}	2.237832×10^{-2}	0.4
160	8.414255×10^{-2}	2.237762×10^{-2}	0.4
320	8.414239×10^{-2}	2.237753×10^{-2}	0.4

TABLE 2. Neutral eigenvalues with decreasing step size: $m = 1$, $\rho = 1$ and $R_e = 800$.

determined by the dimensional speeds U_0, V_0, W_0 so that Δ is known and hence the depth $d = D/\Delta$ can be deduced.

The results of our linear stability analysis are in excellent agreement with those of Hall *et al.* (1984) when the fluid properties are matched across the interface (see figures 3 and 4). For a given wavenumber k, we calculate the Reynolds number which gives neutral stability. In the absence of suction or blowing, our numerical scheme yields the critical values $(R_e)_c = 583.14$, $k_c = 0.2881$ in agreement with Hall *et al.* For $R_e < (R_e)_c$ disturbances are damped and decay to zero exponentially in time. At points inside the neutral curve, the boundary layer is susceptible to travelling wave instabilities which propagate along the attachment line.

An additional check on the numerical results is given by halving the step size used in the finite difference calculations. Table 2 illustrates the accuracy of the scheme as the number of mesh points is doubled.

For a single fluid (corresponding to the case when the fluid properties are matched), suction and blowing have opposite effects on the flow stability. As $\kappa(>0)$ is increased, the critical Reynolds number decreases, and the flow is linearly destabilized by a smaller crossflow velocity. See for example, the neutral curves in figure 3 with $\kappa = 0.137$ and $\kappa = 0.4$, and the results given by Hall *et al.* (1984). Suction, however, can be a useful laminar flow control. The stabilization induced by negative normal velocity at the surface increases the critical Reynolds number, as illustrated by the representative case $\kappa = -0.1$ in figure 3. We have also calculated neutral stability results for other values of κ (namely $\kappa = -0.15, -0.2, -0.25$). In each of these cases the flow is stable over the range $0 < R_e < 1500$ illustrated in figure 3. The asymptotic results of Hall *et al.* show that as $\kappa \to -\infty$, $(R_e)_c$ can be made arbitrarily large. This however, does not take into account the effects of nonlinearity. Hall & Malik (1986) showed that solutions bifurcate subcritically from the upper branch of the neutral curve. The linearly stabilizing role of suction may therefore be destroyed by nonlinearity and transition may be enhanced by the unstable nonlinear modes.

Upon introducing a viscosity and density difference across the interface, the results of the linear stability analysis are significantly altered. For the flow of air over water (the fluid properties are given in table 1), we have obtained results in the cases of both blowing and suction at the wall. With a positive normal velocity at the porous plate, we have chosen the representative cases: $\kappa = 0.027$, $\kappa = 0.04$, and $\kappa = 0.137$. These neutral curves are illustrated in figure 5(*a*). To emphasize the interfacial effect, we have also included the curve (broken line) corresponding to the neutral stability of a single fluid (see figure 3). These eigenvalues were calculated by following the results given by fluids with matched physical properties, and gradually introducing viscosity and density stratification across the interface. As m and ρ increase, the interfacial mode destabilizes the flow. For any given Reynolds number, the band of unstable wavelengths is significantly increased. The upper and lower branches of the neutral curve open out and the critical Reynolds number decreases. For example, with $\kappa = 0.137$ and $D = 6.0$, we obtain critical values $k_c = 0.499$ and $(R_e)_c = 97.81$, whereas for matched fluids the critical values corresponding to $\kappa = 0.137$ are $k_c = 0.309$ and $(R_e)_c = 315.12$.

With suction at the wall, the viscosity and density stratification across the interface also leads to destabilization and the flow is again unstable for a wider band of wavenumbers. In figure 5(*b*) we show neutral curves for the cases $\kappa = -0.1026$ and $\kappa = -0.208$ which correspond to water depths $D = 1.0$ and $D = 0.5$ respectively (see figure 2*a*). With a non-dimensional water depth of 1.0, the flow is unstable even for small Reynolds numbers. Accurate numerical experiments yield critical values $(R_e)_e = 10.9887$, $k_c = 0.7946$. When the depth of the water layer is reduced (and consequently the suction parameter is increased) the critical Reynolds number increases along with the corresponding wavenumber. For example, with $D = 0.5$, we obtain $(R_e)_e = 82.0096$, $k_c = 1.4410$. It is clear then that the usual stabilizing effect of suction at the plate has been negated by the strongly destabilizing influence of the viscosity and density discontinuities at the interface.

A comparison between the theoretical and experimental results is difficult. As discussed earlier, in-flight calculations and wind tunnel experiments indicate that a water layer on the wing surface can have a detrimental effect on drag and lift. This is most likely due to the premature transition from laminar to turbulent flow. The interfacial travelling wave instability observed here is a possible contributing factor in this process. However, experimental investigations into the instability of superposed

fluids have had limited success in quantifying the interfacial mode. Charles & Lilleleht (1965) and Kao & Park (1972) studied the plane Poiseuille flow of oil and water in a channel. They found instability at large Reynolds numbers which appears to arise in the water layer and causes the interface to become wavy. It is not clear that this instability is caused by the interfacial effects; it is more likely that the presence of unstable Tollmien–Schlichting waves in the less-viscous fluid (water) are being observed at the interface. This mode is present at high Reynolds numbers in the absence of a second fluid and is perhaps the one observed experimentally because it has the largest growth rate. More successful experimental results have been obtained for two-fluid flows in cylindrical geometries, where travelling waves are often observed at the interface. The books by Joseph & Renardy (1993) give a good review of recent experimental and theoretical investigations.

The flow described here is a crude model of the actual flow of air over water on swept wings. To make qualitative comparisons between the theoretical calculations and observable phenomenon would require a more sophisticated model in which nonlinear effects are taken into account. The methods adopted by Hall & Malik (1986) could be applied to the two-fluid problem in an analogous manner, although the nonlinear interfacial conditions would complicate the analysis. In addition, global methods could be used to calculate the complete set of eigenvalues, relating the interfacial effects with other modes of instability.

4. Inviscid stationary modes

We now investigate the stationary instability of two-phase flow of air above water over a swept wing, when the Reynolds number is large. As before, we regard the flow in each region as a small perturbation to the basic state. The normal coordinate must now be scaled on the Reynolds number, so that the fluid velocity and pressure are

$$(XU, V, W)_{j=1,2} = \left(X\overline{U}_j, R_e^{1/2}\overline{V}_j, \overline{W}_j\right)\left(YR_e^{1/2}\right) + \delta\left(X\widetilde{U}_j, \widetilde{V}_j, \widetilde{W}_j\right)(X, Y, Z), \tag{20}$$

$$P_{j=1,2} = -\frac{1}{2}\left(\frac{U_0 X \Delta R_e}{W_0}\right)^2 + \frac{\overline{P}_j}{R_e} + \delta\widetilde{P}_j. \tag{21}$$

After substituting (20) and (21) into the non-dimensional Navier–Stokes equations and taking $\delta \to 0$, we recover the ordinary differential system (6)–(7) and boundary conditions (8)–(12) which determine the basic state. At next order the equations governing the linearized stability of the lower fluid layer are

$$\overline{U}_2\frac{\partial\left(X^2\widetilde{U}_2\right)}{\partial X} + X\overline{V}_2\frac{\partial\widetilde{U}_2}{\partial Y} + XR_e^{1/2}\widetilde{V}_2\frac{\partial\overline{U}_2}{\partial Y} + X\overline{W}_2\frac{\partial\widetilde{U}_2}{\partial Z} + \frac{1}{\rho}\frac{\partial\widetilde{P}_2}{\partial X} = \frac{\nu}{R_e}\nabla^2\left(X\widetilde{U}_2\right), \tag{22a}$$

$$X\overline{U}_2\frac{\partial\widetilde{V}_2}{\partial X} + \overline{V}_2\frac{\partial\widetilde{V}_2}{\partial Y} + \widetilde{V}_2\frac{\partial\overline{V}_2}{\partial Y} + \overline{W}_2\frac{\partial\widetilde{V}_2}{\partial Z} + \frac{R_e^{1/2}}{\rho}\frac{\partial\widetilde{P}_2}{\partial Y} = \frac{\nu}{R_e}\nabla^2\widetilde{V}_2, \tag{22b}$$

$$X\overline{U}_2\frac{\partial\widetilde{W}_2}{\partial X} + \overline{V}_2\frac{\partial\widetilde{W}_2}{\partial Y} + R_e^{1/2}\widetilde{V}_2\frac{\partial\overline{W}_2}{\partial Y} + \overline{W}_2\frac{\partial\widetilde{W}_2}{\partial Z} + \frac{1}{\rho}\frac{\partial\widetilde{P}_2}{\partial Z} = \frac{\nu}{R_e}\nabla^2\widetilde{W}_2, \tag{22c}$$

$$\widetilde{U}_2 + \frac{\partial\widetilde{U}_2}{\partial X} + R_e^{1/2}\frac{\partial\widetilde{V}_2}{\partial Y} + \frac{\partial\widetilde{W}_2}{\partial Z} = 0, \tag{22d}$$

where

$$\nabla^2(\cdot) = \frac{\partial^2(\cdot)}{\partial X^2} + R_e\frac{\partial(\cdot)}{\partial Y^2} + \frac{\partial^2(\cdot)}{\partial Z^2}.$$

The corresponding equations for the upper layer are obtained by replacing ρ and ν by unity in the above equations.

Following the inviscid instability theory of Gregory *et al.* (1953) we expect the perturbations to the velocity, pressure and interface to have the following modal expansions, with wavelengths scaled on the boundary layer thickness:

$$\left(X\tilde{U}_j, \tilde{V}_j, \widetilde{W}_j\right) = \left(XU_j, V_j, W_j\right)(Y)\exp\left(\mathrm{i}R_e^{1/2}\left[\int^X \alpha \mathrm{d}X + \beta Z\right]\right), \tag{23a}$$

$$\left(\tilde{\eta}, \tilde{P}_j\right) = \left(\eta, P_j\right)(Y)\exp\left(\mathrm{i}R_e^{1/2}\left[\int^X \alpha \mathrm{d}X + \beta Z\right]\right). \tag{23b}$$

In particular we consider a flow which is neutrally stable so that the wavenumbers α and β are real. As $R_e \to \infty$, an inviscid zone will develop with depth $O\left(R_e^{-1/2}\right)$. This inviscid region is asymptotically matched onto a viscous wall layer so that the no-slip conditions can be satisfied at $Y = -D$. By balancing inertial and viscous terms in equations (22*a–d*), we see that this viscous layer has thickness $O\left(R_e^{-2/3}\right)$. The inviscid perturbations U_j, V_j, W_j and P_j and wavenumbers α and β are then expanded in powers of $O\left(R_e^{-1/6}\right)$:

$$\begin{aligned}
U_j &= U_{j0} + R_e^{-1/6}U_{j1} + \cdots,\\
V_j &= V_{j0} + R_e^{-1/6}V_{j1} + \cdots,\\
W_j &= W_{j0} + R_e^{-1/6}W_{j1} + \cdots,\\
P_j &= P_{j0} + R_e^{-1/6}P_{j1} + \cdots,\\
\alpha &= \alpha_0 + R_e^{-1/6}\alpha_1 + \cdots,\\
\beta &= \beta_0 + R_e^{-1/6}\beta_1 + \cdots.
\end{aligned}$$

Substitution of the neutral disturbances (23*a, b*) into equations (22*a–d*) yields the following leading-order system of equations which govern the inviscid stability of perturbations to the upper and lower fluids when the Reynolds number is asymptotically large:

$$\mathrm{i}X\overline{\overline{U}}_jU_{j0} + XV_{j0}\overline{U}'_j = -\frac{\mathrm{i}\alpha_0 P_{j0}}{\rho}, \tag{24a}$$

$$\mathrm{i}\overline{\overline{U}}_jV_{j0} = -\frac{P'_{j0}}{\rho}, \tag{24b}$$

$$\mathrm{i}\overline{\overline{U}}_jW_{j0} + V_{j0}\overline{W}'_j = -\frac{\mathrm{i}\beta_0 P_{j0}}{\rho}, \tag{24c}$$

$$\mathrm{i}\alpha_0 XU_{j0} + V'_{j0} + \mathrm{i}\beta_0 W_{j0} = 0, \tag{24d}$$

$$\alpha_0 X\overline{U}_{j0} + \beta_0\overline{W}_{j0} = \overline{\overline{U}}_{j0}. \tag{24e}$$

Eliminating U_{j0}, W_{j0} and P_{j0} from equations (24*a–e*) we see that V_{j0} satisfies Rayleigh's

equation, in each layer as follows:

$$\overline{\overline{U}}_1 \left(V_{10}'' - \gamma_0^2 V_{10}\right) = \overline{\overline{U}}_1'' V_{10}, \qquad Y \in [0, \infty), \tag{25a}$$

$$\overline{\overline{U}}_2 \left(V_{20}'' - \gamma_0^2 V_{20}\right) = \overline{\overline{U}}_2'' V_{20}, \qquad Y \in [-D, 0], \tag{25b}$$

$$V_{10}(\infty) = 0, \tag{25c}$$

$$V_{20}(-D) = 0, \tag{25d}$$

$$V_{20}(0) = V_{10}(0), \tag{25e}$$

$$V_{20}'(0) = V_{10}'(0) + \frac{(1-m)\, V_{10}(0)\, \overline{\overline{U}}_{10}'(0)}{m \overline{\overline{U}}_{10}(0)}. \tag{25f}$$

Here $\overline{\overline{U}}_j$ is the 'equivalent' two-dimensional velocity profile, and $\gamma_0^2 = \alpha_0^2 + \beta_0^2$ is the 'effective' wavenumber. Note that the continuity of stresses at the interface is satisfied trivially in the limit as $R_e \to \infty$. The inviscid solution V_{20} is matched onto the viscous perturbation in the wall layer, and in view of the continuity equation (22*d*) this perturbation is $O\left(R_e^{-1/2}\right)$, hence V_{20} satisfies the boundary condition (25*d*).

The point at which $\overline{\overline{U}}_j = 0$ is denoted by $Y = Y_0$, and as Y approaches this value, U_0 and W_0 behave like $1/(Y - Y_0)$. By careful choice of α_0/β_0, $\overline{\overline{U}}_j''$ is also made to vanish as $Y \to Y_0$, so that V_0 has no such singularity, and a classical critical layer analysis is not necessary (see Hall 1986).

4.1. *Asymptotic solution for similar fluids*

The above system may be solved numerically; to do this a suitable initial guess must be made for the eigenvalue γ_0. To assist the location of this eigenvalue, we first consider the analogous problem where the two fluids have equal densities, and the viscosity ratio is close to unity, that is $m = 1 + \epsilon$, where $\epsilon \ll 1$. This case corresponds to the flow of two fluids with similar properties; this is a useful indication of the manner in which the interfacial effects can alter the stability of the flow.

The basic flow and wavenumbers are then expanded in an asymptotic series as

$$\alpha_0 = \alpha_{00} + \epsilon\alpha_{01} + \cdots, \quad \beta_0 = \beta_{00} + \epsilon\beta_{01} + \cdots,$$

$$\gamma_0 = \gamma_{00} + \epsilon\gamma_{01} + \cdots, \quad \gamma_{01} = \frac{\alpha_{00}\alpha_{01} + \beta_{00}\beta_{01}}{\gamma_{00}},$$

$$\overline{U}_j = \overline{U}_{j0} + \epsilon\overline{U}_{j1} + \cdots, \quad \overline{V}_j = \overline{V}_{j0} + \epsilon\overline{V}_{j1} + \cdots,$$

$$\overline{W}_j = \overline{W}_{j0} + \epsilon\overline{W}_{j1} + \cdots, \quad \overline{\overline{U}}_j = \overline{\overline{U}}_{j0} + \epsilon\overline{\overline{U}}_{j1} + \cdots,$$

$$\overline{\overline{U}}_{j0} = \alpha_{00} X \overline{U}_{j0} + \beta_{00} \overline{W}_{j0},$$

$$\overline{\overline{U}}_{j1} = \alpha_{00} X \overline{U}_{j1} + \beta_{00} \overline{W}_{j1} + \alpha_{01} X \overline{U}_{j0} + \beta_{01} \overline{W}_{j0}.$$

The leading-order basic flow in each layer $j = 1, 2$ satisfies

$$\overline{V}_{j0}''' = \overline{V}_{j0}\overline{V}_{j0}'' - \left(\overline{V}_{j0}'\right)^2 + 1, \quad \overline{W}_{j0}'' = \overline{V}_{j0}\overline{W}_{j0}'.$$

$$\overline{V}_{10}'(\infty) = -1, \quad \overline{W}_{10}(\infty) = 1,$$

$$\overline{V}_{20}(-D) = \kappa, \quad \overline{V}_{20}'(-D) = 0, \quad \overline{W}_{20}(-D) = 0,$$

with $\overline{V}_j, \overline{V}_j', \overline{V}_j'', \overline{W}_j$, and $\overline{W}_j'$ continuous at $Y = 0$.

At $O(\epsilon)$,

$$\overline{V}_{11}''' = \overline{V}_{10}\overline{V}_{11}'' - 2\overline{V}_{10}'\overline{V}_{11}' + \overline{V}_{11}\overline{V}_{10}'', \quad \overline{V}_{21}''' = \overline{V}_{20}\overline{V}_{21}'' - 2\overline{V}_{20}'\overline{V}_{21}' + \overline{V}_{21}\overline{V}_{20}'' - \overline{V}_{10}'',$$
$$\overline{W}_{11}'' = \overline{V}_{10}\overline{W}_{11}' + \overline{V}_{11}\overline{W}_{10}', \quad \overline{W}_{21}'' = \overline{V}_{20}\overline{W}_{21}' + \overline{V}_{11}\overline{W}_{10}' - \overline{W}_{20}',$$
$$\overline{V}_{11}'(\infty) = 0, \quad \overline{W}_{11}(\infty) = 0, \quad \overline{V}_{21}'(-D) = 0, \quad \overline{W}_{21}(-D) = 0,$$
$$\overline{V}_{11}(0) = 0 = \overline{V}_{21}(0), \quad \overline{V}_{11}'(0) = \overline{V}_{21}'(0),$$
$$\overline{V}_{11}''(0) = \overline{V}_{21}''(0) + \overline{V}_{20}''(0),$$
$$\overline{W}_{11}(0) = \overline{W}_{21}(0), \quad \overline{W}_{11}'(0) = \overline{W}_{21}'(0) + \overline{W}_{20}'(0).$$

To solve the above equations numerically, we require the asymptotic form of the $O(\epsilon)$ correction to the basic flow as $Y \to \infty$. This is obtained in a manner similar to the derivation of equations (13*a–c*). We find that

$$\overline{V}_{11} = \tau_1 + \Gamma_1\chi - \tau_1\Gamma_0\chi',$$
$$\overline{W}_{11} = -\left(\lambda_1\left(\frac{1}{\xi} + \Sigma\right) + \tau_1\lambda_0\right)\exp\left(-\tfrac{1}{2}\xi^2\right),$$

where τ_1, Γ_1 and λ_1 are constants to be found. The equations governing the basic state were then solved numerically and the results compared with the solution of equations (6)–(7), choosing a value of m close to unity. The results we obtained gave excellent agreement up to $O(\epsilon^2)$.

The solution of (25) may be obtained by solving the adjoint set of equations (see Coddington & Levinson 1955). We recollect that if M is an ordinary differential operator over a region N, the adjoint problem is defined by

$$\int_N \Psi M(\Phi)\,\mathrm{d}y = \int_N \Phi M^+(\Psi)\,\mathrm{d}y = 0.$$

In our case the region $N = [-D, \infty)$, contains two sub-regions $[-D, 0]$ and $[0, \infty)$. This, however, does not present a difficulty: following the work of Blennerhassett (1980) we define a vector

$$\boldsymbol{Z} = \begin{cases} \boldsymbol{Z}_1, & 0 \leqslant Y < \infty, \\ \boldsymbol{Z}_2, & -D \leqslant Y \leqslant 0, \end{cases}$$

and a 2×2 real matrix $\boldsymbol{S}$ such that

$$\boldsymbol{S} = \begin{cases} \boldsymbol{S}_1, & 0 \leqslant Y < \infty, \\ \boldsymbol{S}_2, & -D \leqslant Y \leqslant 0. \end{cases}$$

For upper and lower fluids ($j = 1, 2$ respectively), $\boldsymbol{Z}_j$ and $\boldsymbol{S}_j$ are then chosen such that

$$\boldsymbol{Z}_j = \begin{pmatrix} V_{j0} & \\ V_{j0}' - \dfrac{V_{j0}\overline{\overline{U}}_j'}{\overline{\overline{U}}_j} & \end{pmatrix}, \qquad \boldsymbol{S}_j = \begin{pmatrix} \dfrac{\overline{\overline{U}}_j'}{\overline{\overline{U}}_j} & 1 \\ \gamma_{00}^2 & -\dfrac{\overline{\overline{U}}_j'}{\overline{\overline{U}}_j} \end{pmatrix}.$$

Equations (25a, b) may then be written in vector form $\boldsymbol{Z}' = \boldsymbol{S}\boldsymbol{Z}$, where V_{j0} satisfies no-slip at the boundaries and $\boldsymbol{Z}$ is continuous across the interface. The adjoint problem is now defined by

$$\int_{-D}^{\infty} (\boldsymbol{Z}^+)^T [\boldsymbol{Z}' - \boldsymbol{S}\boldsymbol{Z}] \, \mathrm{d}Y = \left[(\boldsymbol{Z}^+)^T \boldsymbol{Z}\right]_{-D}^{\infty} - \int_{-D}^{\infty} \boldsymbol{Z}^T \left[(\boldsymbol{Z}^+)' + \boldsymbol{S}^T \boldsymbol{Z}^+\right] \mathrm{d}Y = 0.$$

Writing $\boldsymbol{S}^+ = -\boldsymbol{S}^T$ the adjoint system becomes

$$(\boldsymbol{Z}^+)' = \boldsymbol{S}^+ \boldsymbol{Z}^+,$$

where the adjoint function $\boldsymbol{Z}^+$ is also continuous across the interface, and V_{j0}^+ satisfies no-slip at the boundaries. The problem is self-adjoint.

We now perturb the viscosity ratio about $m = 1$, and write

$$V_{j0} = V_{j00} + \epsilon V_{j01} + \cdots,$$
$$\boldsymbol{S}_j = \boldsymbol{S}_{j0} + \epsilon \boldsymbol{S}_{j1} + \cdots,$$
$$\boldsymbol{Z}_j = \boldsymbol{Z}_{j0} + \epsilon \boldsymbol{Z}_{j1} + \cdots.$$

Substitiution into the Rayleigh equations in each fluid layer yields

$$\boldsymbol{Z}_{j0} = \begin{pmatrix} V_{j00} \\ V'_{j00} - \dfrac{V_{j00}\overline{\overline{U}}'_{j0}}{\overline{\overline{U}}_{j0}} \end{pmatrix},$$

$$\boldsymbol{Z}_{j1} = \begin{pmatrix} V_{j01} \\ V'_{j01} - \dfrac{V_{j01}\overline{\overline{U}}'_{j0}}{\overline{\overline{U}}_{j0}} + \dfrac{V_{j00}\left[\overline{\overline{U}}'_{j0}\overline{\overline{U}}_{j1} - \overline{\overline{U}}_{j0}\overline{\overline{U}}'_{j1}\right]}{\overline{\overline{U}}^2_{j0}} \end{pmatrix},$$

$$\boldsymbol{S}_{j0} = \begin{pmatrix} \dfrac{\overline{\overline{U}}'_{j0}}{\overline{\overline{U}}_{j0}} & 1 \\ \gamma_{00}^2 & -\dfrac{\overline{\overline{U}}'_{j0}}{\overline{\overline{U}}_{j0}} \end{pmatrix},$$

$$\boldsymbol{S}_{j1} = \begin{pmatrix} \dfrac{\overline{\overline{U}}'_{j1}\overline{\overline{U}}_{j0} - \overline{\overline{U}}'_{j0}\overline{\overline{U}}_{j1}}{\overline{\overline{U}}^2_{j0}} & 0 \\ 2\gamma_{00}\gamma_{10} & -\left[\dfrac{\overline{\overline{U}}'_{j0}\overline{\overline{U}}_{j1} - \overline{\overline{U}}'_{j1}\overline{\overline{U}}_{j0}}{\overline{\overline{U}}^2_{j0}}\right] \end{pmatrix}.$$

Neglecting terms of $O(\epsilon^2)$, it follows that the momentum equations are

$$O(1): \qquad \boldsymbol{Z}'_0 - \boldsymbol{S}_0 \boldsymbol{Z}_0 = 0, \tag{26}$$

$$O(\epsilon): \qquad \boldsymbol{Z}_1' - \boldsymbol{S}_0 \boldsymbol{Z}_1 = \boldsymbol{S}_1 \boldsymbol{Z}_0. \tag{27}$$

Vectors $\boldsymbol{Z}_0$ and $\boldsymbol{Z}_1$ remain continuous across the interface and V_{j00} and V_{j01} satisfy the no-slip conditions at $Y = -D$ and as $Y \to \infty$. For equation (27) to have a solution, the forcing term on the right-hand side must be orthogonal to the adjoint function, hence

$$\int_{-D}^{0} (\boldsymbol{Z}_{20}^{+}) \boldsymbol{S}_{21} \boldsymbol{Z}_{20} \mathrm{d}Y + \int_{0}^{\infty} (\boldsymbol{Z}_{10}^{+}) \boldsymbol{S}_{11} \boldsymbol{Z}_{10} \mathrm{d}Y = 0.$$

After some manipulation we obtain

$$2\gamma_{00}\gamma_{01} I_0 = -\frac{V_{100}^2(0)\,\overline{\overline{U}}_{10}'(0)}{\overline{\overline{U}}_{10}(0)} - I_1 - I_2, \tag{28a}$$

$$I_0 = \int_{-D}^{0} V_{200}^2 \,\mathrm{d}Y + \int_{0}^{\infty} V_{100}^2 \,\mathrm{d}Y, \tag{28b}$$

$$I_1 = \int_{0}^{\infty} \frac{V_{100}^2 \left[\overline{\overline{U}}_{11}'' \overline{\overline{U}}_{10} - \overline{\overline{U}}_{11} \overline{\overline{U}}_{10}''\right]}{\overline{\overline{U}}_{10}^2} \,\mathrm{d}Y, \tag{28c}$$

$$I_2 = \int_{-D}^{0} \frac{V_{200}^2 \left[\overline{\overline{U}}_{21}'' \overline{\overline{U}}_{20} - \overline{\overline{U}}_{21} \overline{\overline{U}}_{20}''\right]}{\overline{\overline{U}}_{20}^2} \,\mathrm{d}Y. \tag{28d}$$

The integrands of I_1 and I_2 are regular since the singularity at $Y = Y_0$ is removable, for details see Coward (1994). We are now able to calculate γ_{01}, the $O(\epsilon)$ correction to the effective wavenumber, by finding a numerical solution to the leading-order momentum equations (26) and the solvability condition (28*a*).

4.2. *Discussion*

The Rayleigh equations (25*a*, *b*) and associated boundary and interface conditions (25*c*–*f*) describe the inviscid stationary modes of the two-phase flow with general viscosity ratio m and density ratio ρ. These equations were integrated using a standard finite difference method so that for given m and ρ the eigenvalue γ_0 was calculated to a high degree of accuracy.

Figure 6 illustrates the dependence of γ_0^2 upon the lower to upper fluid viscosity ratio for $0.8 \leqslant m \leqslant 24$. The eigenvalue is a strictly increasing function for $m > 0$. The effect of density stratification is more subtle, since it does not appear explicitly in equations (25*a*–*f*), but manifests itself through the calculation of the basic flow.

In the absence of a discontinuity in viscosity across the interface, the wavenumber of the inviscid stationary mode is

$$\gamma_0^2 = \gamma_{00}^2 = 1.4899.$$

Using the asymptotic methods for $m-1 \ll 1$, we obtain the leading-order correction to γ_0 due to a small viscosity difference across the interface. The solvability condition (28*a*) represents two simultaneous equations to determine unknowns α_{01} and β_{01} (taking real and imaginary parts of (28*a*)). However, it is more useful to evaluate

$$\gamma_{01} = \frac{\alpha_{00}\alpha_{01} + \beta_{00}\beta_{01}}{\gamma_{00}}.$$

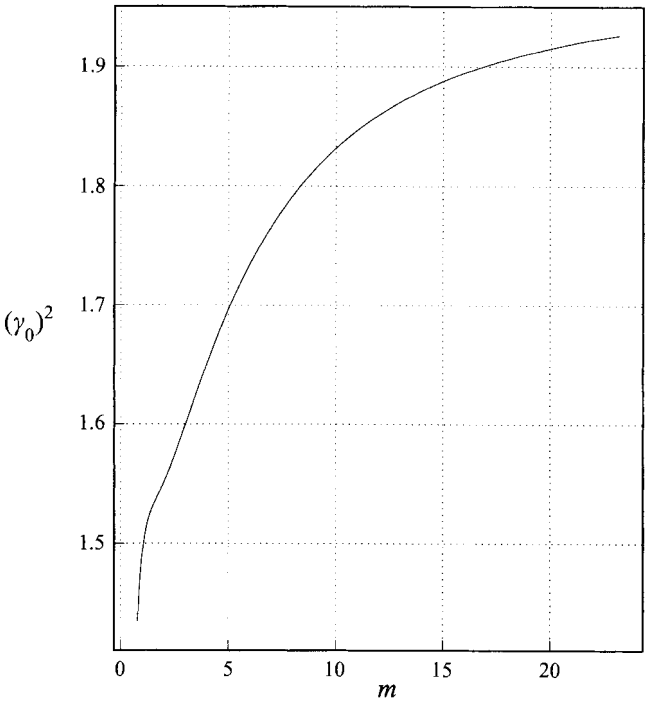

FIGURE 6. Eigenvalues γ_0 as a function of viscosity ratio m.

We find that

$$\gamma_0^2 = \gamma_{00}^2 + 2\epsilon\gamma_{00}\gamma_{01} + O(\epsilon^2),$$
$$= 1.4899 + 0.1726\epsilon + O(\epsilon^2).$$

Figure 7 shows the value of γ_0^2 evaluated using the numerical scheme for m close to unity. The broken line represents the calculation of $\gamma_{00}^2 + 2(m-1)\gamma_{00}\gamma_{01}$ by the asymptotic methods described above.

The eigenvectors illustrated in figures 8(a) and 8(b) have been normalized so that their maximum values are 1.0. Figure 8(a) shows $\overline{V}_{10}$ and $\overline{V}_{20}$ when the two fluids are identical. We notice that the maximum velocity perturbation is at $Y = 0.0839$. Figure 8(b), however, corresponds to the case $m = 5$. Although the velocity perturbation is still continuous, a discontinuity in the first derivative at the unperturbed interface position has developed due to the equation of tangential stress continuity. The maximum of $\overline{V}_{10}$ now occurs much further away from the interface, at $Y = 1.341$.

The orientation of the disturbances relative to the streamwize axis is determined by the wave angle Φ such that

$$\frac{\alpha_0}{\beta_0} = \frac{\alpha_{00}}{\beta_{00}} + \frac{\alpha_{01}\beta_{00} - \alpha_{00}\beta_{01}}{\beta_{00}^2}\epsilon + O(\epsilon^2),$$
$$= 0.7514 + 37.88\epsilon + O(\epsilon^2),$$
$$= \tan\left[\tfrac{1}{2}\pi - \Phi\right].$$

For matched fluid properties the effective wavenumber and wave angle given above correspond to the single-fluid case. As viscosity stratification is introduced, we obtain the above corrections to these quantities and these in turn are in agreement with our numerical results for general viscosity and density ratios. These calculations are

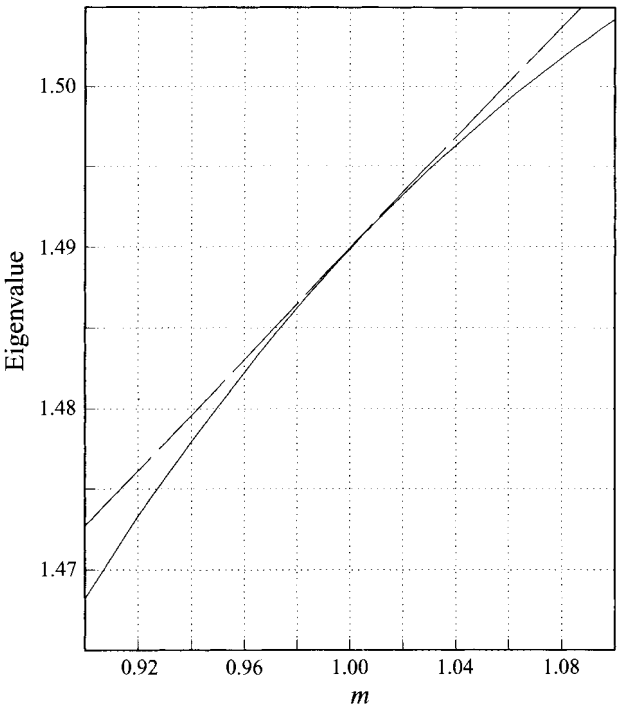

FIGURE 7. Eigenvalue γ_0 for similar fluids: a comparison of asymptotic and numerical results when the viscosity ratio m is close to unity.

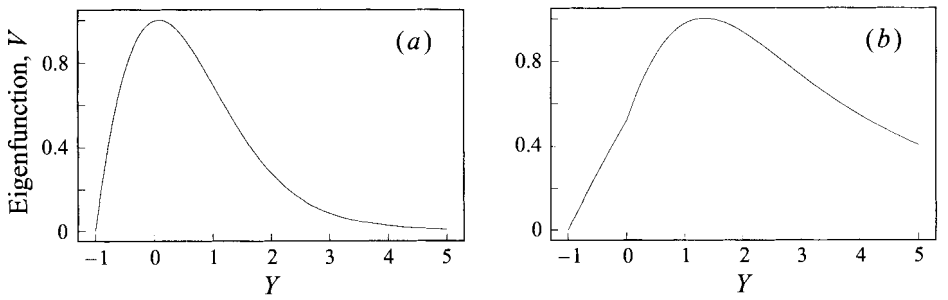

FIGURE 8. Eigenfunction: (*a*) equal densities and viscosities; (*b*) equal densities, viscosity ratio $m = 5.0$.

based on an infinite-Reynolds-number assumption. This work could be extended to include viscous effects in an analogous manner to the method used by Hall (1986) for the flow over a rotating disk. Viscous effects enter at $O\left(R_e^{-1/16}\right)$; the corresponding momentum equations must then be solved to determine $U_{j1}, V_{j1}, W_{j1}, \ldots$, and the solutions matched onto the inviscid flow. The analysis is, however, made more difficult due to the complicated interfacial conditions which match the flow across the two regions.

5. Conclusions

In §§3 and 4 we have considered both two- and three-dimensional disturbances to the flow of air over water. The exact solution of the Navier–Stokes equations described

in §2 is a crude model of the flow near the leading edge of a swept wing during heavy rainfall. We have shown that the interfacial forces have a significant effect on the stability of the attachment-line flow. Viscous travelling waves are predicted at lower Reynolds numbers than is the case for air flow in the absence of a second fluid. The instability is due to the discontinuity in the viscosity and density across the interface between the two fluid regions and occurs with either blowing or suction at the plate.

At infinitely large Reynolds numbers, the interface also alters the neutral stability of stationary modes of the form considered by Gregory *et al.* (1953). The three-dimensional basic flow is written in terms of an 'equivalent' two-dimensional velocity profile which has an inflection point when the velocity is zero. Consequently the critical layer is passive and the ensuing calculations of the eigenvalues and eigenvectors for three-dimensional disturbances follow in a straightforward manner. Using both general numerical methods and asymptotic techniques for the flow of similar fluids we have obtained the corrections to the disturbance wavenumber and orientation due to interfacial effects.

This research was supported by the National Aeronautics and Space Administration under NASA Contract No. NAS1-19480 while the authors were in residence at the Institute for Computer Applications in Science and Engineering (ICASE), NASA Langley Research Center, Hampton, VA 23681-0001. This work was also supported by the Science and Engineering Research Council.

REFERENCES

BATCHELOR, G. K. 1967 *An Introduction to Fluid Dynamics.* Cambridge University Press.

BLENNERHASSETT, P. J. 1980 The generation of waves by wind. *Phil. Trans. R. Soc. Lond.* A **298**, 451–493.

CHARLES, M. E. & LILLELEHT, L. U. 1965 An experimental investigation of stability and interfacial waves in co-current flow of two liquids. *J. Fluid Mech.* **22**, 217–224.

CODDINGTON, E. A. & LEVINSON, N. 1955 *Theory of Ordinary Differential Equations.* McGraw-Hill.

COWARD, A. V. 1994 The stability of two-phase flows. PhD Thesis, University of Manchester, UK.

DUNHAM, D. J., DUNHAM, R. E., JR. & BEZOS, G. M. 1991 A summary of NASA research on effects of heavy rain on airfoils. *AGARD Rep.* 496.

FEDEROV, B. I., PLAVNIK, G. Z., PROKHOROV, I. V. & ZHUKHOVITSKII, L. G. 1976 Transitional flow conditions on a rotating disc. *J. Engng Phys.* **31**, 1448–1453.

GASTER, M. 1967 On the flow along swept leading edges. *Aero. Q.* **18**, 165–184.

GREGORY, N., STUART, J. T. & WALKER, W. S. 1953 On the stability of three-dimensional boundary layers with application to the flow due to a rotating disk. *Phil. Trans. R. Soc. Lond.* A **248**, 155–199.

HALL, P. 1986 An asymptotic investigation of the stationary modes of instability of the boundary layer on a rotating disc. *Proc. R. Soc. Lond.* A **406**, 93–106.

HALL, P. & MALIK, M. R. 1986 On the instability of a three dimensional attachment-line boundary layer; weakly nonlinear theory and a numerical approach. *J. Fluid Mech.* **163**, 257-282.

HALL, P., MALIK, M. R. & POLL, D. I. A. 1984 On the stability of an infinite swept attachment line boundary layer. *Proc. R. Soc. Lond.* A **395**, 229–245.

HEURRE, P. & MONKEWITZ, P. A. 1990 Local and global instabilities in spatially developing flows. *Ann. Rev. Fluid Mech.* **22**, 473–537.

HOOPER, A. P. 1985 Long-wave instability at the interface between two viscous fluids: thin layer effects. *Phys. Fluids* **28**, 1613–1618.

HOOPER, A. P. & BOYD, W. G. C. 1983 Shear-flow instability at the interface between two viscous fluids. *J. Fluid Mech.* **128**, 507–528.

HOOPER, A. P. & BOYD, W. G. C. 1987 Shear-flow instability due to a wall and a viscosity discontinuity at the interface. *J. Fluid Mech.* **179**, 201–225.

JOSEPH, D. D. & RENARDY, Y. Y. 1993 *Fundamentals of Two-Fluid Dynamics*, Vols. 1 & 2. Springer.

KAO, T. W. & PARK, C. 1972 Experimental investigations of the stability of channel flows. Part 2. Two-layered co-current flow in a rectangular region. *J. Fluid Mech.* **52**, 401–423.

MALIK, M. 1986 The neutral curve for stationary disturbances in rotating-disk flow. *J. Fluid Mech.* **164**, 275–287.

MALIK, M. R., CHUANG, S. & HUSSAINI, M. Y. 1982 Accurate numerical solution of compressible, linear stability equations. *Z. Angew. Math. Phys.* **33**, 189–201.

PFENNINGER, W. & BACON, J. W. 1969 *Viscous Drag Reduction* (ed. C. S. Wells), pp. 85–105. Plenum.

POLL, D. I. A. 1979 Transition in the infinite swept attachment line boundary layer. *Aero. Q.* **30**, 607–628.

POLL, D. I. A. 1980 In *IUTAM Symp. on Laminar-Turbulent Transition, Stuttgart.* Springer.

PRANDTL, L. 1946 On boundary layers in three-dimensional flow. *Rep. Aero Res. Coun., Lond. No.* 9828.

RENARDY, Y. Y. 1985 Instability at the interface between two shearing fluids in a channel. *Phys. Fluids* **28**, 3441–3443.

ROSENHEAD, L. (ed.) 1963 *Laminar Boundary Layers.* Oxford University Press.

SEARS, W. R. 1948 The boundary layer of yawed cylinders. *J. Aero. Sci.* **15**, 49–52.

YIH, C. S. 1967 Instability due to viscosity stratification. *J. Fluid Mech.* **27**, 337–352.